



The effect of starting material types on the structure of graphene oxide and graphene

Filiz BORAN^{1,*}, Sevil ÇETİNKAYA GÜRER²

¹Department of Chemical Engineering, Faculty of Engineering, Hitit University, Çorum, Turkey

²Department of Chemical Engineering, Faculty of Engineering, Cumhuriyet University, Sivas, Turkey

Received: 23.01.2019

Accepted/Published Online: 25.07.2019

Final Version: 07.10.2019

Abstract: In this study, the effects of starting material types on graphene oxide (GO) are reported with the aim of developing graphene (GR) synthesis. The GOs were prepared from natural graphite (NG) powder and graphite nanoplate (GNp) based on the Hummers method. Two kinds of GR were successfully synthesized using GOs, which were prepared from NG and GNp in the presence of hydrazine and ammonia for 24 h at a 100 °C reaction temperature. The synthesized GOs and GRs were characterized by X-ray diffraction (XRD) techniques, Fourier transform infrared, high-contrast transmission electron microscopy (HCTEM), dispersive Raman spectroscopic analyses, and elemental analyses. HCTEM analyses of GOs and GRs exhibited largely folded, convoluted, and entwined GO and GR structures. The XRD and Raman analyses showed that the number of layers of GO1, GO2, GR1, and GR2 were 9.27, 13.53, 4.11, and 5.26, respectively. On the other hand, GR1, prepared from NG powder, showed much higher quality (peak intensities (I_D/I_G) = 1.53, C/O = 3.64) than GR2, which was prepared from GNp (I_D/I_G = 1.64, C/O = 3.17). Thus, this study provides a way to produce higher quality GOs and GRs.

Key words: Hummers method, graphene, graphene oxide, graphite nanoplate, thermal shocking

1. Introduction

Graphite structures can be viewed as stacked 2-dimensional hexagonal carbon material and are used to create single or multilayer graphene (GR), as well as its derivatives, such as graphene oxide (GO). GR is a monolayer of these structures in a honeycomb lattice, which has been considered to be a building block because it is wrapped to form fullerenes, rolled to form carbon nanotubes, or stacked regularly to form graphite [1–4]. GR and GO layers have been investigated effectively to form new composite materials. Due to the unique properties of the components of the composites, these new nanomaterials have great potential in various applications, such as catalysts, enzyme adsorption, cell imaging, and drug delivery [5,6].

A literature review indicated the 6 most commonly used methods reported to prepare GR. These are: 1) the micromechanical exfoliation method [7], 2) the chemical vapor deposition method [8], 3) epitaxial growth (top-seed growth) [9], 4) longitudinal unzipping of carbon nanotubes [10,11], 5) organic synthesis routes [12], and 6) colloidal suspension of graphite or graphite derivatives [13]. GR is prepared via the reduction and modification of GO for use in nanocomposite materials. Methods for the oxidation of graphite to GO include the Brodie, Staudenmaier, and Hummers methods, as well as some minor modifications of some of these methods [14]. At present, the traditional Hummers method is the primary method for preparing GO. Graphite is often chosen

*Correspondence: filizbektas@hitit.edu.tr

as the starting material because of its low price and availability [15,16]. Although there have been numerous studies on the synthesis of GO, the effect of graphite type as a starting material on the structural properties of the synthesized GO and GR has been very scarcely reported [17,18]. Botas et al. reported the influence of 2 different parent graphites, which were obtained from identical fractions of coal under different conditions, on the structure of GO [19]. Jankovsky et al. compared the significant differences between individual GRs prepared using different GOs as starting materials. They prepared 5 types of GOs using the Brodie, Hofmann, Hummers, Staudenmair, and Tour methods, and then different GR materials were synthesized via the chemical and thermal reduction of these 5 types of GOs [17]. Yokwana et al. prepared nitrogen-doped graphene oxide (NGO) nanosheets via a 1-pot modified Hummers method, using either graphite powder or graphite flakes as starting materials without any pretreatment such as grinding, thermal shocking and, chemical process. Their study showed that the NGO produced from 2 different starting materials possessed different properties and adsorption performances. In addition, it was obtained with different starting materials to produce NGO with different N and O contents, thus playing a critical role in controlling the morphological and structural properties, and the surface area of the NGO [20]. Çelik et al. prepared a few layers of GR via the exfoliation of 3 types of graphite, expandable graphite (EG) (grade 3772), surface-enhanced flake graphite (SEFG) (grade 3725), and high surface flake graphite (primary artificial (PA)-grade TC307), as the starting materials. Only one study in the literature has reported synthesized GR using starting materials of different sizes. However, they used commercial surface-enhanced flake graphite [3].

The purpose of this work was to examine the effect of using 2 different graphite samples (NG and graphite nanoplate (GNP) reproduced from the NG) as starting materials on the structure of GO and GR. In addition, this study attempted to bring about further understanding of the pretreatment options which include thermal shocking and ultrasonic treatment of graphite after interaction with strong acids for synthesizing GO and GR. The chemical composition of the synthesized products was investigated via elemental analyses. The structural properties were investigated using X-ray diffraction (XRD), Fourier transform infrared (FTIR), high-contrast transmission electron microscopy (HCTEM), and dispersive Raman spectroscopic analyses. The synthesized products were also compared in terms of the number of layers and quality.

2. MATERIALS AND METHODS

2.1. Materials

Commercial natural graphite (NG), sulfuric acid (H_2SO_4 , 98%), nitric acid (HNO_3 , $\geq 65\%$), hydrochloric acid (HCl, 37%), sodium nitrate (NaNO_3), potassium permanganate (KMnO_4), hydrogen peroxide (H_2O_2 , 35%), hydrazine monohydrate (N_2H_4), ammonia solution (NH_3 , 26%), and ethyl alcohol were all purchased from Sigma-Aldrich (Sigma, St. Louis, MO, USA) as analytical grade materials without further purification.

2.2. Methods

2.2.1. Preparation of the GNP

A mixture of H_2SO_4 (80 mL) and HNO_3 (20 mL) in 100 mL (4:1) was added to 2 g of graphite and the mixture was stirred for 16 h. Next, it was washed with water until a pH of 7 was reached, and then it was dried at 100 °C. After thermal shocking at 1050 °C, the resulting product was subjected to ultrasonic treatment for 8 h by placing it in a 70% solution of 100 mL of ethyl alcohol (Figure 1) [21,22]. The synthesized sample was named GNP.

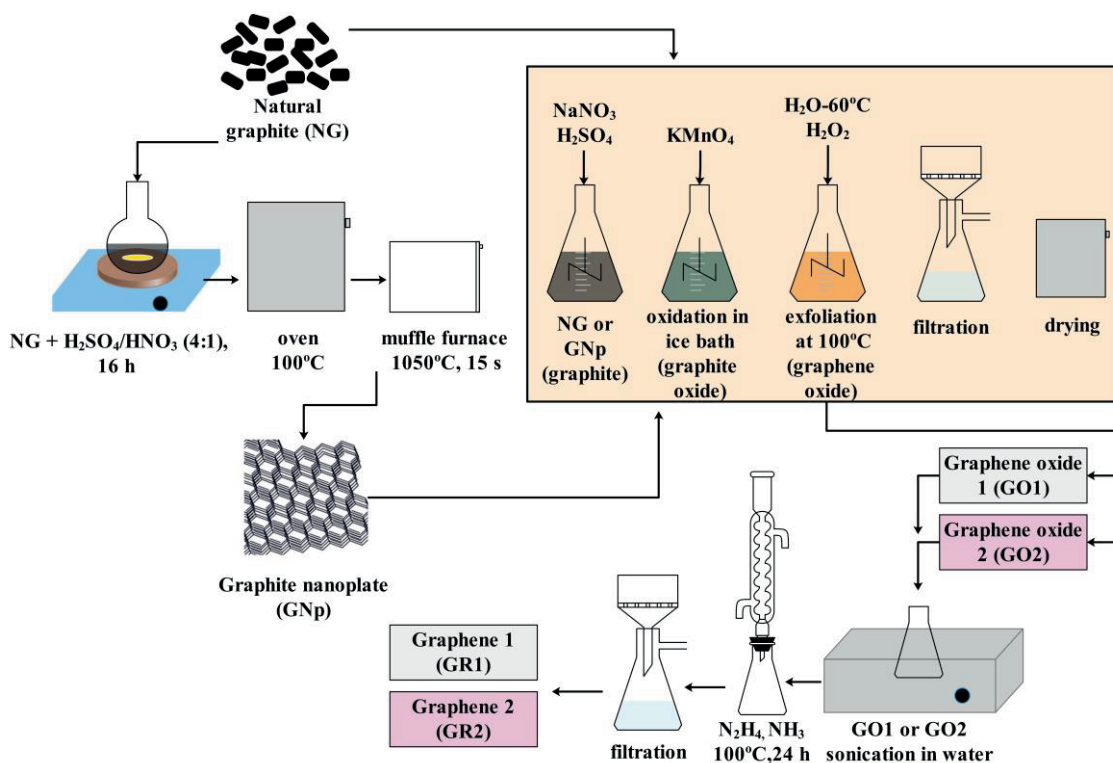


Figure 1. Schematic representation of GR synthesis procedures starting with NG and GNP.

2.2.2. Preparation of the GO

After adding 2 g of NG and 1 g of NaNO_3 to a glass ball in an ice bath, 46 mL of concentrated H_2SO_4 was slowly added to the mixture. Next, the mixture was stirred for 30 min and 6 g of KMnO_4 was added to the mixture. After stirring the mixture for several minutes, 92 mL of water at 60°C was added to it. H_2O_2 was then added to stop the oxidation until bubbles were no longer seen. The mixture was held at approximately 100°C for 1 h, filtered by shaking, and washed 3–4 times with 5% HCl and then with deionized water until $\text{pH} \sim 7$ (Figure 1). This procedure was repeated using GNP instead of NG as the starting material. As shown in Figure 1, the prepared GOs using NG and GNP were labeled GO1 and GO2, respectively.

2.2.3. Preparation of the graphene (GR)

The previously prepared GO materials were dispersed in 250 mL of water for 1 h in sonication. Certain amounts of hydrazine monohydrate and NH_3 were added to the mixture while stirring the mixture at 100°C for 24 h in an oil bath in a water-cooled condenser. Next, the mixture was filtered and washed with 5×100 mL of water and 5×100 mL of ethanol (Figure 1). The GR materials prepared using GO1 and GO2 were labeled as GR1 and GR2, respectively.

2.2.4. Characterization

The characterization of the synthesized materials was performed using XRD, FTIR (Thermo Scientific/Nicolet IS50), and HCTEM (FEI, Tecnai G2 Spirit Biotwin Model, operated at an accelerating voltage of 20–120 kV). Dispersive Raman spectroscopic analyses were also carried out utilizing the Thermo/DXR Raman Instrument

(532 nm laser excitation). Elemental composition was determined from elemental analyses using a Thermo Finnigan Flash EA 1112 series elemental analyzer.

3. Results and Discussion

The FTIR spectra of the NG and GNp are shown in Figure 2a. The broad peak observed at 3425 cm^{-1} corresponded to the O-H groups of the hydroxyl and carboxyl groups in all of the samples [23]. Moreover, the peak at 1629 cm^{-1} may be attributed to the O-H bending vibration (Figure 2a) [24]. The peak seen at 1731 cm^{-1} in the FTIR spectra of all of the graphite samples showed the C = O vibration in the carboxylic acid or carbonyl moieties (Figures 2a and 2b) [25]. After exfoliation of the NG, the intensity of these peaks in the GNp spectra decreased due to fragmentation into foliated. After reduction of the GO samples, this band almost disappeared owing to the removal of oxygen chemical groups [26]. In the spectra of GR1 and GR2, the small binary peaks at 2842 and 2917 cm^{-1} correspond to the symmetrical and antisymmetrical -CH₂- vibrations [16]. The absorption peak at around 1560 cm^{-1} observed in the graphite could be attributed to the benzene rings (Figure 2c) [27]. No differences were observed in the FTIR spectra of either GR sample.

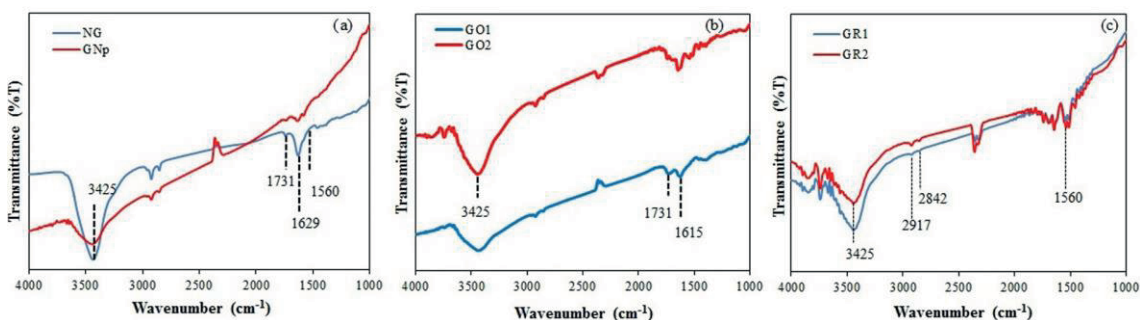


Figure 2. FTIR spectrum of (a) NG and GNp, (b) GO1 and GO2, and (c) GR1 and GR2.

The XRD patterns of the NG, GNp, GOs, and GRs are presented in Figure 3. The characteristic peaks of the NG and GNp were observed at or around $2\theta = 26.6^\circ$ and 55.6° (Figure 3) [28]. Moreover, the XRD spectrum of the GNp indicated that there was no change in the galleries of the carbon layers during sonication and that the strong peak at around $2\theta = 26.6^\circ$ of the intercalation did not occur in the spaces between the carbon layers during production. The diffraction peaks seen in the NG and GNp at $2\theta = 26.6^\circ$ disappeared on the whole once the GO or GR was synthesized (Figure 3).

The XRD diffractograms of GO1 and GO2 are shown in Figure 3. The graphite-specific sharp peak at around $2\theta = 26.6^\circ$ became a weak broad peak in GO1 and disappeared in GO2. Furthermore, the strong peak at around $2\theta = 12.5^\circ$ in GO1 and small peak at around $2\theta = 11.3^\circ$ in GO2 indicated wider interstitial spaces [23].

The XRD diffraction peaks of GO1 ($2\theta = 12.5^\circ$) and GO2 ($2\theta = 11.3^\circ$) disappeared in GR1 and GR2 and the broad peaks at $2\theta = 25.4^\circ$ appeared in the spectrum of the GR samples (Figure 3). This suggested that GO can be reduced to GR during the hydrothermal reaction [29]. It can be clearly seen that this peak was slightly wider in GR2 than in GR1. This could be attributed to the formation of wider interstratified voids originating from the use of GNp as the starting material in GR2 [23]. Since HNO₃ is a common oxidizing agent used to react via an aromatic carbon surface, it was used for preparing the GNp. After thermal shocking, the applied sonication ensured that the graphite particles were fragmented and foliated, and GNp was formed [30].

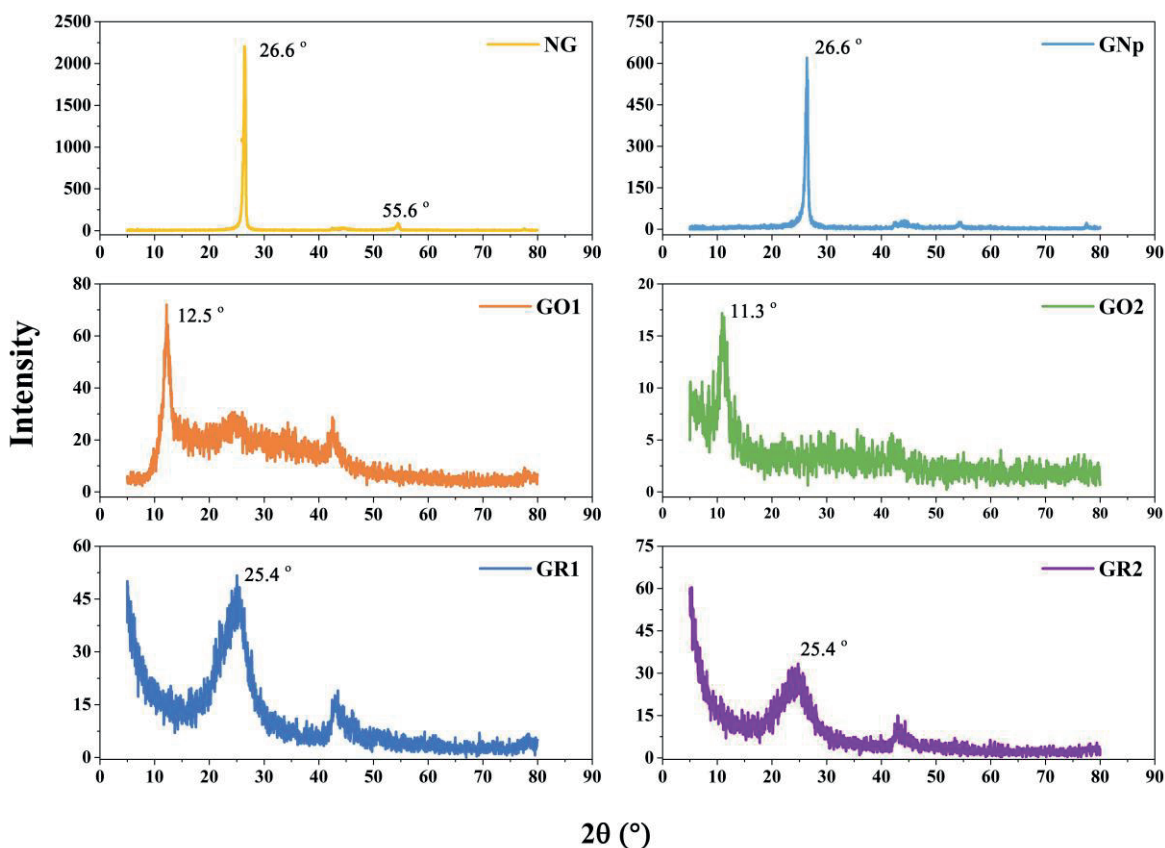


Figure 3. XRD patterns of NG, GNp, GO1, GO2, GR1, and GR2.

Due to all of these pretransactions, the use of foliated graphite as a starting material when synthesizing GR resulted in wider interstratified voids.

For all of the synthesized samples, first, the interlayer distances (d) between the planes were determined using Bragg's law, as given in Eq. (1) [31]. Next, the crystal size of the XRD spectroscopy (002) plane was calculated using the Scherrer equation given in Eq. (2). The number of layers was also calculated according to Eq. (3), by proportioning the crystal size (D_p) and d -distance between the layers [32,33].

$$n\lambda = 2d\sin\theta \quad (1)$$

$$D_p = \frac{K\lambda}{\beta\cos\theta} \quad (2)$$

$$\text{Number of layers} = \frac{D_p}{d} \quad (3)$$

Here, D_p is the average size of the particles, K is the Scherrer constant (0.94), β is the full width at half maximum of the XRD peak, n is a constant (1), λ is the XRD wavelength (Cu $K\alpha$ average = 1.54178 Å), and θ is the XRD peak position (one half of 2θ) [31,33].

As shown in Table 1, the d -distance was determined as 0.335 nm for the NG and GNp, while it was 0.708 and 0.782 nm for GO1 and GO2, respectively. This result could exhibit the oriented layer structure of

the graphite. In addition, the interlayer distance increased from 0.335 nm to 0.708 and 0.782 nm after chemical oxidation. The increased spacer distance between these carbon planes was due to the intercalation of the oxygen functional groups and water molecules. Furthermore, the interlayer d-spacing for GR1 and GR2 decreased to 0.35 nm, which could be attributed to the removal of the oxygen functional groups [34]. From Table 1, it can be seen that the number of layers for the NG (67.46) and GNp (52.09) was larger than that of GO1 (9.27) and GO2 (13.53), and the number of layers for GR1 (4.11) and GR2 (5.26) decreased from 10 to around 4 or 5 when compared to the GO samples.

Table 1. X-ray structural parameters for all of the samples studied in this study.

Samples	2 Theta	d (nm)	Dp (nm)	Dp/d (number of layers)
NG	26.6	0.335	22.6	67.46
GNp	26.6	0.335	17.45	52.09
GO1	12.5	0.708	6.56	9.27
GO2	11.3	0.782	10.58	13.53
GR1	25.4	0.35	1.44	4.11
GR2	25.4	0.35	1.84	5.26

Raman spectroscopy is an effective analysis method to study the electronic structure of materials and hence was used to evaluate the quality of the synthesized GR-based materials [35,36]. Figure 4 shows the Raman spectra of the NG and GNp, while Figures 5 and 6 show the Raman spectra of the 2 GO and 2 GR samples, respectively. The G band can be ascribed to the ordered sp^2 carbon, while the D band can be ascribed to the disordered carbon, edge defects, and other defects (sp^3 bonded carbon, dangling bonds, and vacancies) [23]. This situation is clearly shown in Figures 4, 5, and 6, as the peaks centered at the G band ($\sim 1575\text{ cm}^{-1}$) and D band ($\sim 1311\text{ cm}^{-1}$) of the GR-based materials were attributed to ordered sp^2 bounded carbon atoms in a 2-dimensional hexagonal lattice and edge defects of the chemically reduced GR sheets, respectively [16].

Table 2 shows the Raman peak positions of the D and G bands and their D/G intensity ratios, which gives a measure of the quality of the samples. The D/G intensity ratios are also given in Figure 7. Chemically reduced GO from the NG and GNp exhibited peaks at 1633 and 1588 cm^{-1} (G band), respectively. The peaks at 1324 and 1314 cm^{-1} (D band) showed the characteristic defects and disorders of GO1 and GO2 sheets, respectively. A comparison of the ratios of the 2 peak intensities (I_D/I_G) showed the quality of the samples. As the ratios came close to zero, the carbon atoms had a more ordered structure [37]. The increase in D/G was attributed to the production of defects in the carbon cages by displacement or spraying of the carbon atoms, while the decrease in D/G was linked to the structure restoration [26]. The I_D/I_G values were 1.53 and 1.64 for GR1 and GR2, respectively. These results illustrated that the structure of GR1 had fewer defects than the structure of GR2. The differences between the structures of GR1 and GR2 may be related to the use of different starting materials while synthesizing them.

Table 3 demonstrates the elemental composition and C/O atomic ratios calculated from the elemental analyses for all of the samples. The elemental analysis results were used to determine the degree of reduction of the GO samples, and the C/O atomic ratios are also given in Figure 8. The C/O atomic ratios of the GO samples were about 1.19 and 1.08, which includes the contribution of the H_2O molecules retained in the GO particles [38]. The C/O atomic ratios for the NG and GNp decreased from 7.33 to 1.19 for GO1 and from 5.06 to

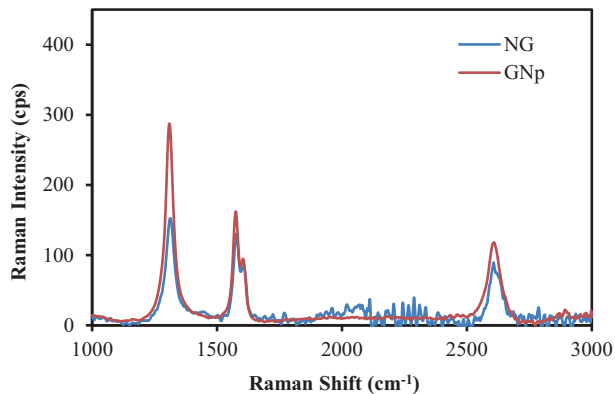


Figure 4. Raman spectra of the NG and GNp.

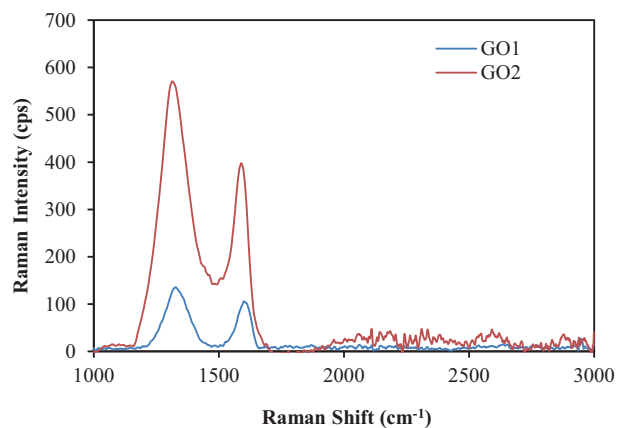


Figure 5. Raman spectra of GO1 and GO2.

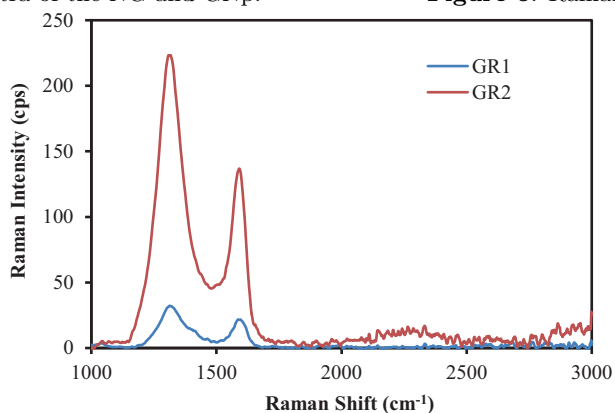


Figure 6. Raman spectra of GR1 and GR2.

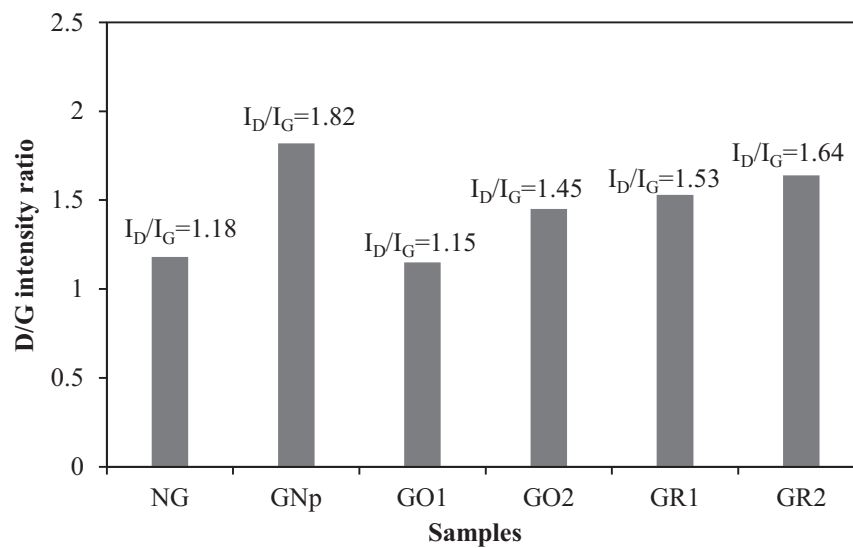
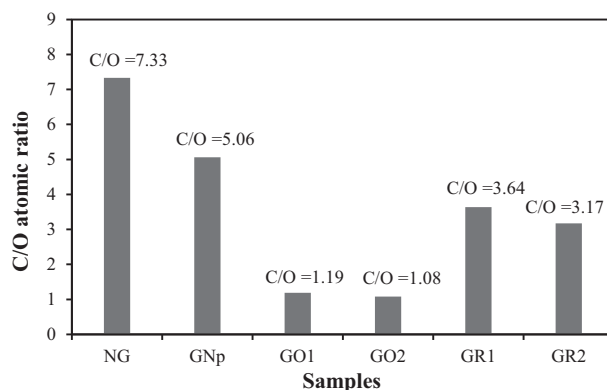


Figure 7. D/G Raman intensity ratios.

Table 2. Raman peak positions and D/G intensity ratios for all of the samples.

Sample name	D band (cm^{-1})	G band (cm^{-1})	I_D/I_G
NG	1311.46	1575.66	1.18
GNp	1308.57	1574.69	1.82
GO1	1323.99	1633.51	1.15
GO2	1313.39	1588.19	1.45
GR1	1309.53	1581.44	1.53
GR2	1309.53	1588.19	1.64

1.08 for GO2, respectively. This decrease was due to the oxidation of graphite to GO. Later on, the C/O atomic ratios for GO1 and GO2 increased from 1.19 to 3.64 for GR1 and from 1.08 to 3.17 for GR2, respectively. This increase could be related to the reduction of GO to GR due to the removal of the oxygenated groups during the chemical reduction [38,39]. The increase of the C/O atomic ratio also indicated that the reduction period of the GO to GR was improved [40]. The results showed that the use of GNp instead of NG as the starting material slightly affected the reduction of the GO to GR, removal of the oxygen-containing functional groups, and regular graphite lattice restoration. Moreover, the degree of reduction of GR1 was greater than that of GR2 [38]. These data obtained by the elemental analyses support the results of the XRD and Raman analyses. There was a correlation between the number of GR layers and the degree of graphite exfoliation. A decrease in the number of layers indicated a high degree of exfoliation [17]. According to the sum of all results obtained here, the highest degree of reduction and exfoliation was observed in GR1, which was synthesized from GO originating from NG.

**Figure 8.** C/O atomic ratio from the elemental analysis for all samples.

The C/O ratio and number of layers are important parameters for GR-based materials [41]. These important parameters of the GR-based materials obtained in this study are compared with the literature in Table 4. Jankovsk et al. [17] pointed out the significant differences between chemically reduced GRs prepared using different GOs, which were synthesized by the Hummers (HU), Brodie (BR), and Staudenmaier (ST) techniques. The numbers of layers of the obtained GR samples in this study were similar to the chemically reduced GR prepared using GO synthesized by the HU method and lower than that of GR prepared using GO synthesized by the BR and ST techniques. However, the C/O atomic ratios for GR1 and GR2 were close to those of the BR and ST techniques and lower than that of the HU method. Moreover, Çelik et al. [3] presented

Table 3. Elemental composition of all samples from the elemental analysis.

Sample name	C (%)	O (%)	C/O ratio
NG	87.99	12.01	7.33
GNp	83.54	16.46	5.06
GO1	54.24	45.76	1.19
GO2	51.85	48.15	1.08
GR1	78.45	21.55	3.64
GR2	76.01	23.99	3.17

significant differences between GR thin films prepared using different graphites, which were EG, SEFG, and PA in isopropyl alcohol (IPA). They reported that few-layer GR (3–5), prepared from EG by thermal treatment of expandable graphite, exhibited higher quality ($I_D/I_G < 0.09$). However, they did not examine the C/O ratios. As a result, high-quality GR in the current study was synthesized directly from NG, without any pretreatments, according to the chemical and thermal reduction studies of GR in the literature.

Table 4. Comparison of the elemental composition ratios, XRD, and Raman features of the obtained GR products with the literature.

Sample name	I_D/I_G	Number of layers	C/O ratio	Reference
*HU-CRG	1.17	3	10.11	[17]
*BR-CRG	1.11	10	4.29	[17]
*ST-CRG	1.09	6–7	5.73	[17]
**EG-IPA-90 min-TS	0.07	3–5	Untried	[3]
**SEFG-IPA-90 min	0.24	3–5	Untried	[3]
**PA-IPA-90 min	0.30	3–5	Untried	[3]
GR1	1.53	4.11	3.64	Present study
GR2	1.64	5.26	3.17	Present study

*: Chemically reduced GRs prepared using different GOs, which were synthesized conformably to the Hummers (HU), Brodie (BR), and Staudenmaier (ST) techniques. **: GR thin films prepared using different graphites: expandable graphite (EG), surface enhanced flake graphite (SEFG), and primary artificial (PA).

HCTEM images of the NG, GNp, GO1, and GO2 are shown in Figure 9. The HCTEM image of the NG shows the laminar structure of the graphite with dimensions of $> 1 \mu\text{m}$. Moreover, the GNp consisted of thinner graphite nanolamellae at 157 nm in width and 4.2 nm in thickness. As shown in these images, the structures of the NG and GNp had some overlapping parts. On the other hand, the HCTEM micrographs of GO1 and GO2 showed that the sheets were largely folded, convoluted, and entwined with each other. As in the study by Botas et al., no significant difference was observed between the 2 GOs in our study [19]. According to the XRD results, the number of layers obtained for GO1 and GO2 were close to the maximum 10 layers required for an end result of GR structures. This analysis also supported that the GR1 and GR2 HCTEM micrographs (Figure 10) exhibited similar structures to the GO1 and GO2 HCTEM micrographs. However, the nonfolded and nonscrolled edges were only observed for GR1 and the HCTEM micrographs and revealed 4-layer GR only in agreement with the XRD analyses. The HCTEM results supported the fact that corrugation and convolution

were a part of the inherent nature of the GR nanolayers, as reported in the literature [3].

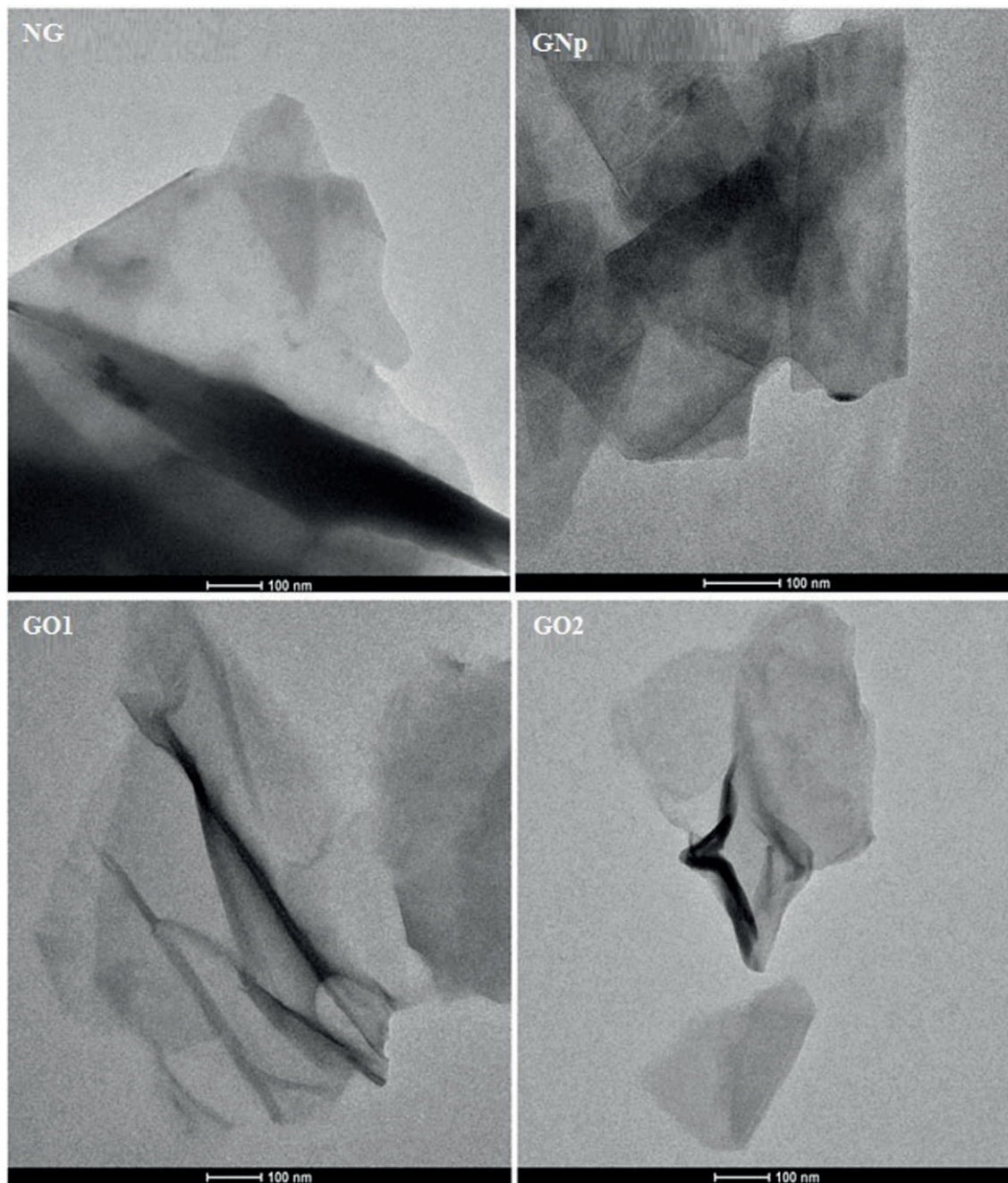


Figure 9. HCTEM images of NG, GNp, GO1, and GO2 (scale bar: 100 nm).

In conclusion, in this study, two different graphite-based materials, NG and GNp, reproduced from NG, were investigated as starting materials for preparing GR. The GOs were successfully prepared from NG and GNp. The XRD results illustrated that changing the type of graphite affected the formation of wider gaps between the layers. The XRD analyses also revealed that GR1 had a decreased crystal size and number of layers when compared with GR2, indicating that more defects existed on the surface. According to the results of the Raman analyses, GR1 prepared from NG exhibited higher quality ($I_D/I_G = 1.53$, $C/O = 3.64$) than

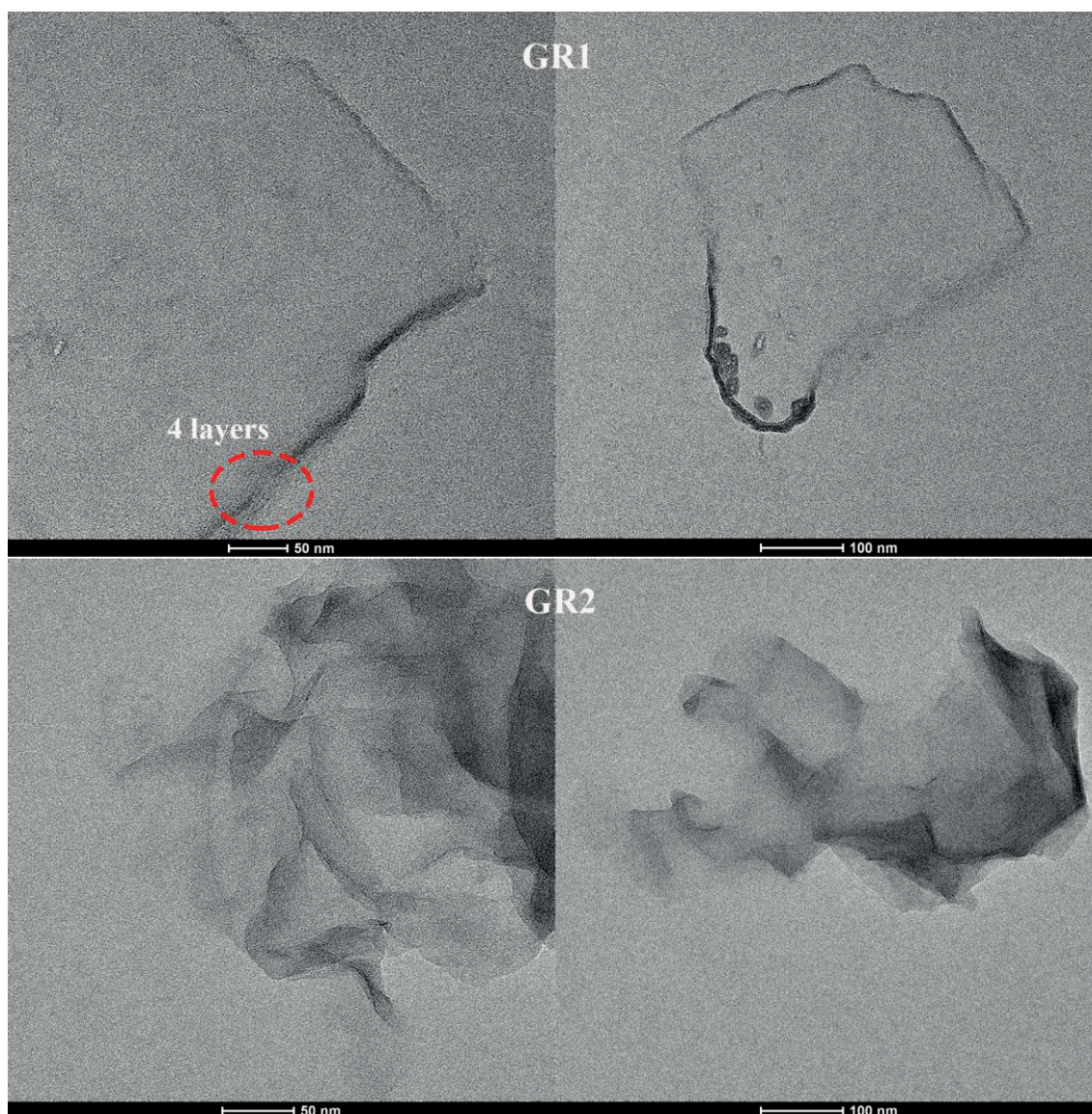


Figure 10. HCTEM images of GR1 and GR2 (scale bar: 50–100 nm).

GR2 prepared from GNp ($I_D/I_G = 1.64$, $C/O = 3.17$). This is good evidence that NG can be used without any pretreatment to prepare GR. The findings showed that the type of graphite used as the starting material to prepare GO and GR influences the resulting GR properties.

Acknowledgment

This work was supported by the Cumhuriyet University Scientific Research Projects Unit (CUBAP) as Project Number M601.

References

1. Saeed K, Khan I. Efficient photodegradation of neutral red chloride dye in aqueous medium using graphene/cobalt–manganese oxides nanocomposite. *Turkish Journal of Chemistry* 2017; 41: 391-398. doi: 10.3906/kim-1606-44

2. Li J, Shi H, Li N, Li M, Li J. Facile preparation of graphite intercalation compounds in alkali solution. *Central European Journal of Chemistry* 2010; 8: 783-788. doi: 10.2478/s11532-010-0048-5
3. Çelik Y, Flahaut E, Suvacı E. A comparative study on few-layer graphene production by exfoliation of different starting materials in a low boiling point solvent. *FlatChem* 2017; 1: 74-88. doi: 10.1016/j.flatc.2016.12.002
4. Sreedhar D, Devireddy S, Veeredhi VR. Synthesis and study of reduced graphene oxide layers under microwave irradiation. *Materials Today Proceedings* 2018; 5: 3403-3410. doi: 10.1016/j.matpr.2017.11.585
5. Ozsoy N, Ozsoy M, Mimaroglu A. Taguchi approach to tribological behaviour of chopped carbon fiber-reinforced epoxy composite materials. *Acta Physica Polonica A* 2017; 132: 846-848. doi: 10.12693/APhysPolA.132.846
6. Wang K, Ruan J, Song H, Zhang J, Wo Y et al. Biocompatibility of graphene oxide. *Nanoscale Research Letters* 2011; 6: 1-8. doi: 10.1007/s11671-010-9751-6
7. Sinclair RC, Suter JL, Coveney PV. Micromechanical exfoliation of graphene on the atomistic scale. *Physical Chemistry Chemical Physics* 2019; 21: 5716-5722. doi: 10.1039/c8cp07796g
8. Yilmaz M, Eker YR. Synthesis of graphene via chemical vapour deposition on copper substrates with different thicknesses. *Anadolu University Journal of Science and Technology A - Applied Sciences and Engineering* 2017; 18 (2): 289-300. doi:10.18038/aubtda.279709
9. Çelebi C, Yanik C, Demirkol AG, Kaya II. The effect of a SiC cap on the growth of epitaxial graphene on SiC in ultra high vacuum. *Carbon* 2012; 50: 3026-3031. doi: 10.1016/j.carbon.2012.02.088
10. Kosynkin DV, Higginbotham AL, Sinitskii A, Lomeda JR, Dimiev A et al. Longitudinal unzipping of carbon nanotubes to form graphene nanoribbons. *Nature* 2009; 458: 872-876. doi: 10.1038/nature07872
11. Rangel NL, Sotelo JC, Seminario JM. Mechanism of carbon nanotubes unzipping into graphene ribbons. *Journal of Chemical Physics* 2009; 131: 1-5. doi: 10.1063/1.3170926
12. Koehler FM, Stark WJ. Organic synthesis on graphene. *Accounts of Chemical Research* 2013; 46: 2297-2306. doi: 10.1021/ar300125w
13. Titelman GI, Gelman V, Bron S, Khalfin RL, Cohen Y et al. Characteristics and microstructure of aqueous colloidal dispersions of graphite oxide. *Carbon* 2005; 43: 641-649. doi: 10.1016/j.carbon.2004.10.035
14. Bai S, Shen X. Graphene-inorganic nanocomposites. *The Royal Society of Chemistry* 2012; 2: 64-98. doi: 10.1039/c1ra00260k
15. Kim J, Cote LJ, Huang J. Two dimensional soft material: new faces of graphene oxide. *Accounts of Chemical Research* 2012; 45: 1356-1364. doi: 10.1021/ar300047s
16. Kuila T, Bose S, Mishra AK, Khanra P, Kim NH et al. Chemical functionalization of graphene and its applications. *Progress in Materials Science* 2012; 57: 1061-1105. doi: 10.1016/j.pmatsci.2012.03.002
17. Jankovský O, Marvan P, Nováček M, Luxa J, Mazánek V et al. Synthesis procedure and type of graphite oxide strongly influence resulting graphene properties. *Applied Materials Today* 2016; 4: 45-53. doi: 10.1016/j.apmt.2016.06.001
18. Wu ZS, Ren W, Gao L, Liu B, Jiang C et al. Synthesis of high-quality graphene with a pre-determined number of layers. *Carbon* 2009; 47: 493-499. doi: 10.1016/j.carbon.2008.10.031
19. Botas C, Álvarez P, Blanco C, Santamaría R, Granda M et al. The effect of the parent graphite on the structure of graphene oxide. *Carbon* 2012; 50: 275-282. doi: 10.1016/j.carbon.2011.08.045
20. Yokwana K, Kuvarega AT, Mhlanga SD, Nxumalo EN. Mechanistic aspects for the removal of Congo red dye from aqueous media through adsorption over N-doped graphene oxide nanoadsorbents prepared from graphite flakes and powders. *Physics and Chemistry of the Earth* 2018; 107: 58-70. doi: 10.1016/j.pce.2018.08.001
21. Chen G, Weng W, Wu D, Wu C. PMMA/graphite nanosheets composite and its conducting properties. *European Polymer Journal* 2003; 39: 2329-2335. doi: 10.1016/j.eurpolymj.2003.08.005

22. Chen G, Wu C, Weng W, Wu D, Yan W. Preparation of polystyrene/graphite nanosheet composite. *Polymer* 2003; 44: 1781-1784. doi: 10.1016/S0032-3861(03)00050-8
23. Liu X, Wu Y, Yang Z, Pan F, Zhong X et al. Nitrogen-doped 3D macroporous graphene frameworks as anode for high performance lithium-ion batteries. *Journal of Power Sources* 2015; 293: 799-805. doi: 10.1016/j.jpowsour.2015.05.074
24. Zhao B, Zhang G, Song J, Jiang Y, Zhuang H et al. Bivalent tin ion assisted reduction for preparing graphene/SnO₂ composite with good cyclic performance and lithium storage capacity. *Electrochimica Acta* 2011; 56: 7340-7346. doi: 10.1016/j.electacta.2011.06.037
25. Kassaei MZ, Motamedi E, Majidi M. Magnetic Fe₃O₄-graphene oxide/polystyrene: fabrication and characterization of a promising nanocomposite. *Chemical Engineering Journal* 2011; 172: 540-549. doi: 10.1016/j.cej.2011.05.093
26. Ansón-Casaos A, Puértolas JA, Pascual FJ, Hernández-Ferrer J, Castell P et al. The effect of gamma-irradiation on few-layered graphene materials. *Applied Surface Science* 2014; 301: 264-272. doi: 10.1016/j.apsusc.2014.02.057
27. Bykkam S, Rao V, Chakra S, Thunugunta T. Synthesis and characterization of graphene oxide and its antimicrobial activity against *Klebsiella* and *Staphylococcus*. *International Journal of Advanced Biotechnology and Research* 2013; 4: 142-146.
28. Yang Y, Qi S, Wang J. Preparation and microwave absorbing properties of nickel-coated graphite nanosheet with pyrrole via in situ polymerization. *Journal of Alloys and Compounds* 2012; 520: 114-121. doi: 10.1016/j.jallcom.2011.12.136
29. Pan S, Liu X. ZnS-Graphene nanocomposite: synthesis, characterization and optical properties. *Journal of Solid State Chemistry* 2012; 191: 51-56. doi: 10.1016/j.jssc.2012.02.048
30. Chen G, Weng W, Wu D, Wu C, Lu J et al. Preparation and characterization of graphite nanosheets from ultrasonic powdering technique. *Carbon* 2004; 42: 753-759. doi: 10.1016/j.carbon.2003.12.074
31. Roy Chowdhury D, Singh C, Paul A. Role of graphite precursor and sodium nitrate in graphite oxide synthesis. *The Royal Society of Chemistry* 2014; 4: 15138-15145. doi: 10.1039/c4ra01019a
32. Yazıcı M, Tiyek İ, Ersoy MS, Alma MH, Dönmez U et al. Synthesis of graphene oxide (GO) by modified Hummers methods and its characterization. *Gazi Üniversitesi Fen Bilim Dergisi Part C Tasarım ve Teknoloji* 2016; 4: 41-48 (in Turkish with an abstract in English).
33. Andonovic B, Temkov M, Ademi A, Petrovski A, Grozdanov A et al. Laue functions model vs. scherrer equation in determination of graphene layers number on the ground of XRD data. *Journal of Chemical Technology and Metallurgy* 2014; 49: 545-550.
34. Loryuenyong V, Totepvimarn K, Eimburanaprat P, Boonchompoo W, Buasri A. Preparation and characterization of reduced graphene oxide sheets via water-based exfoliation and reduction methods. *Advances in Materials Science and Engineering* 2013; 2013: 1-5. doi: 10.1155/2013/923403
35. Thema FT, Moloto MJ, Dikio ED, Nyangiwe NN, Kotsedi L et al. Synthesis and characterization of graphene thin films by chemical reduction of exfoliated and intercalated graphite oxide. *Journal of Chemistry* 2013; 2013: 1-6. doi: 10.1155/2013/150536
36. Min YL, Zhang K, Zhao W, Zheng FC, Chen YC et al. Enhanced chemical interaction between TiO₂ and graphene oxide for photocatalytic decolorization of methylene blue. *Chemical Engineering Journal* 2012; 193-194: 203-210. doi: 10.1016/j.cej.2012.04.047
37. Venkata Ramana G, Padya B, Srikanth VVSS, Jain PK, Padmanabham G et al. Electrically conductive carbon nanopipe-graphite nanosheet/polyaniline composites. *Carbon* 2011; 49: 5239-5245. doi: 10.1016/j.carbon.2011.07.041
38. Park S, An J, Potts JR, Velamakanni A, Murali S et al. Hydrazine-reduction of graphite and graphene oxide. *Carbon* 2011; 49: 3019-3023. doi: 10.1016/j.carbon.2011.02.071
39. Mohanapriya K, Jha N. Fabrication of one dimensional graphene nanoscrolls for high performance supercapacitor application. *Applied Surface Science* 2018; 449: 461-467. doi: 10.1016/j.apsusc.2017.12.186

40. Huang SY, Zhao B, Zhang K, Yuen MMF, Xu JB et al. Enhanced reduction of graphene oxide on recyclable Cu foils to fabricate graphene films with superior thermal conductivity. *Scientific Reports* 2015; 5: 1-11. doi: 10.1038/srep14260
41. Morales-Narváez E, Sgobbi LF, Machado SAS, Merkoçi A. Graphene-encapsulated materials: synthesis, applications and trends. *Progress in Materials Science* 2017; 86: 1-24. doi: 10.1016/j.pmatsci.2017.01.001